Early View publication on www.interscience.wiley.com
(issue and page numbers not yet assigned;
citable using Digital Object Identifier – **DOI**)

phys. stat. sol. (a), 1–9 (2008) / **DOI** 10.1002/pssa.200879731

physica status solidi a
www.pss-a.com
applications and materials science

Hydrogen in nano-diamond films: experimental and computational studies

Sh. Michaelson[1], R. Akhvlediani[1], A. Hoffman[*,1], A. Silverman[2], and J. Adler[3]

[1] Schulich Faculty of Chemistry, Technion – Israel Institute of Technology, Haifa 32000, Israel
[2] Taub Computer Center, Technion – Israel Institute of Technology, Haifa 32000, Israel
[3] Department of Physics, Technion – Israel Institute of Technology, Haifa 32000, Israel

Received 21 April 2008, revised 25 May 2008, accepted 28 May 2008
Published online ■■■

PACS 68.55.Ln, 71.15.Pd, 79.20.Uv, 81.05.Uw, 81.15.Gh

* Corresponding author: e-mail choffman@tx.technion.ac.il, Phone: +972-4-8293747; Fax: 972-4-8295703

We present studies related to the incorporation of hydrogen and its bonding configuration in diamond films composed of diamond grains of varying size which were deposited by three different methods: hot filament (HF), micro wave (MW) and direct current glow discharge (dc GD) chemical vapor deposition. The size of the diamond grains which constitute the films varies in the following way: hundreds of nm in the case of HF CVD ("sub-micron size", ~300 nm), tens of nm in the case of MW CVD (3–30 nm) and a few nm in the case of dc GD CVD ("ultra nano-crystalline diamond", ~5 nm). Secondary ion mass spectroscopy (SIMS) and high resolution electron energy loss spectroscopy (HR-EELS) were applied to investigate the hydrogen trapping in the films. The hydrogen retention of the diamond films increases with decreasing grain size, indicating that most likely hydrogen is bonded and trapped in grain boundaries as well as on the internal grain surfaces. HR-EELS analysis shows that at least part of this hydrogen is bonded to sp^2- and sp^3-hybridized carbon, thus giving rise to typical C–H vibration modes. The vibrational spectroscopies show the increase of sp^2 C–H modes in transition from sub-micron to ultra nano-crystalline grain size. These conclusions are supported by preliminary results of computer simulations which show that hydrogen atoms at the boundary between a nano-diamond particle and an amorphous shell have lower energy than hydrogen atoms within either the nano-diamond or the amorphous region. These results suggest that hydrogen is expected to be localized at the nano-diamond/amorphous carbon interface as experimentally found.

1 Introduction Hydrogen is a key component of the gas mixture usually used for diamond nucleation and growth by chemical vapour deposition (CVD) methods. It is thus involved in many different processes related to diamond nucleation and growth. It is no wonder that hydrogen must be incorporated in some quantity in diamond films and the questions to be asked are: (1) in what quantities, (2) in what locations (in the grains as interstitials, forming defect-H clusters in the grains, on the diamond surfaces, in grain boundaries and in a non-diamond constituent between the grains (e.g. when nano-diamond crystallites are embedded in an a-C/graphitic matrix)), (3) in what bonding configuration. In this paper we summarised and extended our studies related to hydrogen concentration and bonding configuration in diamond films of varying grain size [1–3].

The films consist of diamond crystallites of sizes from a ~5 nm to ~300 nm depending on deposition methods and conditions [4–6]. The thickness of continuous films varies from ~70 nm to ~1000 nm depending on deposition time. The investigated diamond films were grown by three different kinds of CVD methods: (1) hot filament (HF) CVD; (2) direct current glow discharge (dc GD) CVD and (3) MW CVD. The first two methods utilize hydrogen rich gas mixtures (CH_4/H_2 ratio were 1/99 and 9/91 correspondingly), while the third one uses a Ar rich plasma. The three investigated kinds of diamond films, grown by different techniques, have different microstructure and phase composition. Our experimental studies are complemented by a computer simulation study in which the hydrogen bonding to a diamond particle surrounded by an amorphous shell is investigated. To this aim we simulated a model system

consisting of 512 atoms to describe a nano-diamond particle surrounded by an amorphous shell. Hydrogen atoms were introduced into this structure and the total energy of the system was calculated for different hydrogen interstitial sites. We also simulated the dynamics of hydrogen atoms in the nano-diamond/amorphous carbon interface.

The structure of this paper is as follows. In Section 2 we give a brief description of the three different kinds of diamond films investigated in the present work. In Section 3 the hydrogen concentration as a function of diamond grain size studied by secondary ion mass spectroscopy (SIMS) is presented. In Section 4 hydrogen bonding configuration on well defined film surfaces was studied by high resolution electron energy loss spectroscopy (HR-EELS). In Section 5 a brief summary of our recent computational results is presented.

2 Brief description of deposition methods and microstructure of the films Three kinds of CVD diamond films were grown on silicon substrates by different methods. Below the main differences in the deposition method, growth mechanism and film microstructure are briefly discussed.

(1) MW CVD nano-diamond films were grown from a hydrogen poor gas mixture. The films were grown on Si substrates maintained at 800 °C using a microwave power of 1200 W and total gas pressure of 200 Torr. Prior to deposition the silicon substrates were seeded mechanically in solution with diamond powder. Two gas mixtures were used to deposit nanodiamond films: (i) 1.4% CH_4 and 98.6% Ar. In this case the growth rate is 0.96 μm/hours and diamond grain size 3–20 nm (film labelled MW-CVD-3–20 nm); (ii) 1.4% CH4, 1% H_2 and 97.6% Ar. In this case the growth rate is 2.7 μm/hour and grain size 10–30 nm (film labelled MW-CVD-10–30 nm) [6].

The mechanism of the film formation was investigated to a great extent [7] and is considered as a surface process occurring from C_2 molecule as the main growth species. Nano-diamond film growth from C_2 species require a surface pre-treatment aimed to introduce diamond growth centres onto which the film grows. The as-deposited films are characterized by a high sp^3 content of ~95% [7] and nano-metric grain size (in the present study, in the range 3–30 nm), homogeneously distributed over the whole thickness.

(2) HF CVD diamond films were grown from a hydrogen rich gas mixture (CH_4/H_2 ratio was 1/99). The evolution of the film occurs on nucleation centers immersed into the substrate by ultrasonic abrasion with poly-dispersed mixed diamond slurry [5]. This pretreatment results in an initial diamond particle density (DPD) of $\sim 5 \times 10^{10}$ cm^{-2}. This high DPD value allows deposition of continuous films with a minimal thickness of ~70–100 nm [5, 8]. The nucleation is a surface process while the main growth species are CH_x and hydrogen radicals. The diamond growth occurs on nucleation centers, which gradually merge and coalesce into continuous film. The crystal size evolves from ~50–70 nm in the nearly coalescent film (~100 nm film thickness, ~10 min deposition) (Fig. 1A) and reaches nearly a constant value of 300–400 nm in micron thick films (deposition time ~1 hour) (Fig. 1B). The increased crystalline size observed in the high resolution scanning electron microscopy (HR-SEM) images (Fig. 1) is a result of the suppression of small crystallites by fast growing crystallites which comprise the faceted surface. All the deposited films are characterized by high diamond quality (>98% sp^3) and well defined diamond facets.

(3) dc GD CVD films were grown from hydrogen rich plasma (CH_4/H_2 ratio was 9/91) by means of continuous substrate bombardment by positive hydrocarbon and hydrogen ions of ~100–200 eV kinetic energy [9, 10]. No pretreatment procedure is needed to induce diamond nucleation. The nano-diamond nucleation and growth occur in the sub-surface region of the film resulting in the upper surface region consisting of hydrogenated amorphous carbon. The film evolves on top of a hydrogenated carbonaceous precursor containing a mixture of an amorphous and graphitic carbon formed during the first ~20 min of deposition (~300 nm thickness). When the precursor density reaches ~3 g/cm^3, nano-diamond particles precipitate and grow to a final size of ~5 nm by means of preferential displacement of loosely bonded carbon atoms by energetic ions [9, 10]. The sp^3 content of the film grown for 1 hour reaches ~80%. The nano-diamond particles are embedded

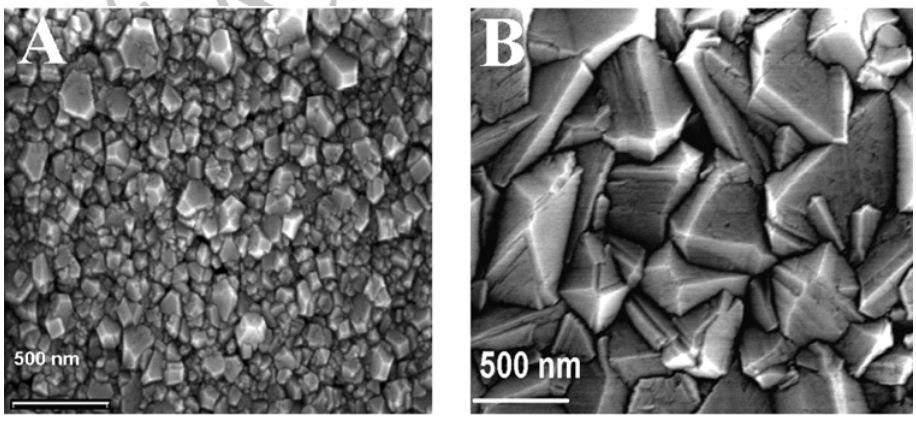

Figure 1 HR-SEM micrographs of as deposited HF CVD diamond films: (A) film deposited from $CH_4 + H_2$ gas mixture for 10 min (thickness ~100 nm, grain size ~50–70 nm); (B) film deposited from $CH_4 + H_2$ gas mixture for 60 min (thickness ~700 nm, grain size ~300 nm).

Table 1 Summary of a grain size and deposition methods of the investigated diamond films.

film name	grain size [nm]	deposition method	gas composition (CH_4/H_2/Ar)
dc-GD-CVD-5 nm [10]	~5	dc glow-discharge CVD	9/91/0
HF-CVD-300 nm [5]	300	hot filament CVD	1/99/0
MW-CVD-3–20 nm [6]	3–20	micro-wave CVD	1.4/0/98.6
MW-CVD-10–30 nm [6]	10–30	micro-wave CVD	1.4/1/97.6

in hydrogenated amorphous carbon matrix. Table 1 summarizes the deposition methods and the resulting grain size of all the investigated diamond films.

3 Hydrogen concentrations in the films as a function of grain size studied by SIMS The hydrogen concentration within the three different kinds of diamond films described above were analysed by SIMS technique [1, 2, 11]. SIMS analysis was carried out in a dynamic mode in a Cameca IMS4f ion microscope using a 14.5 keV Cs^+ ion beam. The sampling area was about 64 μm^2. The basic chamber pressure was 8×10^{-10} Torr, while the ion current was about 1×10^{-8} A.

SIMS depth profiles of hydrogen concentration within the different diamond films are shown in Fig. 2. Profile 2A was measured for a ~1.6 μm thick HF CVD sample grown for 2 hours from $CH_4 + H_2$ gas mixture. Its initial grain size (close to the film-Si substrate interface) is ~50 nm and develops during the deposition to a final grain size of 300–400 nm, thus allowing a direct measurement of the correlation between the hydrogen trapping and the crystalline size. Note, that the sampling depth given in Fig. 2 represents the film surface at a depth of 0 and the Si substrate region at a depth of 1.6 μm. It is very clear that the hydrogen concentration of this film decreases from 6×10^{20} atoms/cm^3 at the region close to the Si substrate (50 nm grain size) to 1.2×10^{20} atoms/cm^3 in the region close to the film's surface formed after a deposition time of ~2 hours (~300 nm grain size) [1, 2, 11].

The profile of hydrogen atoms in dc GD CVD film grown for 1 hour is shown in Fig. 2, curve B. In our previous works [9, 10] we showed that the growth of the dc GD CVD film advances through the following stages: (1) graphitic film with its basal plane perpendicular to the substrate, a low H concentration and low (~2.2 g/cm^3) density, (2) an increase of the density followed by incorporation of hydrogen, (3) the formation of a dense (~3 g/cm^3), hydrogen rich layer in which diamond nucleates and grows. The hydrogen concentration in the nano-diamond film deposited by dc GD CVD increases from 3.3×10^{21} at the nano-graphitic precursor region to 1.45×10^{22} atoms/cm^3 in the ~5 nm sized nano-diamond crystallites region [12]. The hydrogen concentration depth profile of the dc GD film reflects the evolution of its structure from an initial low density, low hydrogen concentration graphitic film through a medium density, hydrogen containing film until a dense, hydrogen containing matrix evolves, in which ~5 nm sized nano-diamond crystallites precipitate. Our previous measurements of absolute hydrogen concentration within these films by means of ERDA revealed hydrogen concentration of 15–20 at% [12] which confirms the present SIMS measurements.

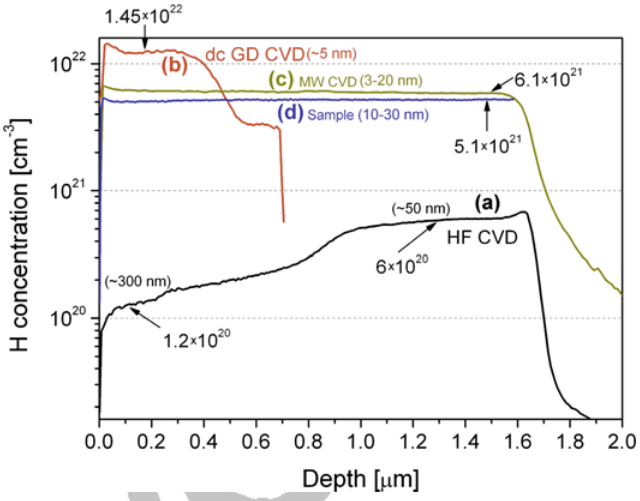

Figure 2 (online colour at: www.pss-a.com) SIMS profile of hydrogen atoms within three different types of diamond films. (A) HF CVD film deposited from $CH_4 + H_2$ gas mixture for 2 hours. Note the decrease of H concentration from 6×10^{20} atoms/cm^3 at initial growth region (grain size ~50 nm) to 1.2×10^{20} H/cm^3 for thicker film (grain size ~300 nm). (B) 700 nm thick nano-diamond film deposited by dc GD CVD. The hydrogen concentration increases from 3.3×10^{21} atoms/cm^3 at the initial stage of film evolution (predominantly graphitic precursor) up to 1.45×10^{22} atoms/cm^3 in the region where ~5 nm sized nano-diamond grains are embedded in an amorphous carbon matrix. (C) MW CVD diamond film with grain size 3–20 nm. (D) MW CVD diamond film with grain size in the range of 10–30 nm.

In Fig. 2, curves C and D show the hydrogen concentration in two nano-diamond films deposited by MW CVD with grain size of 3–20 nm and 10–30 nm, respectively. The measured hydrogen concentration for samples MW-CVD-3–20 nm and MW-CVD-10–30 nm were 6.1×10^{21} atoms/cm^3 and 5.1×10^{21} atoms/cm^3, correspondingly. Note the slightly larger hydrogen concentration in MW-CVD-3–20 nm (CH_4/Ar ratio of 1.4/98.6, grain size 3–20 nm) than in MW-CVD-10–30 nm (CH_4/H_2/Ar ratio of 1.4/1/97.6, grain size 10–30 nm), e.g. despite the higher hydrogen concentration in the gas phase its retention within the film is lower for the last sample. Moreover, the hydrogen concentration in MW CVD films (grown from hydrogen poor gas mixture) largely exceeds that measured for the HF CVD grown films (carried out in a hydrogen rich atmosphere). Therefore, one may suggest that the hydrogen incorporation within the diamond film is governed by another factor beyond gas mixture composition. The

Table 2 Hydrogen concentration versus the crystalline size and the surface to volume atom ratio.

film type	H concentration atoms/cm^3	H concentration (at%)[1]	crystalline size (nm)	surface to volume atom ratio (%)[2]
HF CVD (1 hour)	1.2×10^{20}	0.12	300	0.5
HF CVD (10 min)	6×10^{20}	0.6	50	3
MW-CVD-3–20 nm	6.1×10^{21}	6.1	3–20	50–7.5
MW-CVD-10–30 nm	5.1×10^{21}	5.1	10–30	15–5
dc-GD-CVD-5nm	1.45×10^{22}	14.5	5	28

[1] Assuming a C concentration of 1×10^{23} atoms $\times$ cm^{-3}
[2] Surface to volume atom ratio of FCC crystallite with the same crystalline size

most evident factor which influences the hydrogen atom retention within the films is diamond grain size. Our results clearly show that the smaller diamond crystallites, the higher hydrogen concentration within the films. Note, that all samples were mounted at the same time in the SIMS chamber and measured at the same conditions. Therefore, while the absolute hydrogen concentration values within the films may depend on the correct relative sensitivity factor (RSF), the relative measured concentrations can be compared.

Table 2 summarizes the H concentrations in the different films, the atomic percentage of H (assuming a C density of 10^{23} atoms/cm^3), the crystalline size deduced from HR-SEM and HR-TEM, and the surface to volume atom ratio of FCC crystallites with the same crystalline size. It is very clear that the hydrogen concentration in the diamond films increases with decreasing crystalline size. This result strongly suggests that hydrogen atoms decorate the internal grain interface of the bulk's diamond films. The trapping of hydrogen in grain boundaries is a natural consequence of the accepted diamond growth mechanism which involves adsorption of a CH_x growth species first and then abstraction of one hydrogen atom from the surface by atomic hydrogen in the gas phase, allowing the diamond carbon atom to be bonded to another CH_x radical. Coalescence of adjacent diamond crystallites most likely does not result in complete hydrogen desorption from touching surfaces leading to the incorporation of hydrogen on the touching crystallites surfaces (grain boundaries). In the case of nano-diamond film deposition form energetic species hydrogen stabilizes the nano-diamond grains as discussed in our previous studies [9, 10].

4 Hydrogen bonding configuration on diamond film surface studied by HR-EELS HR-EELS is a most powerful surface characterization probe, which may provide direct information about hydrogen bonding on surfaces [13]. The electron spectroscopy measurements reported in our studies were carried out using an ultra-high vacuum (UHV) system consisting of two chambers connected in tandem. In the first chamber annealing, XPS was carried out, whereas the second chamber is dedicated to HR-EELS. The samples can be heated in-situ up to ~1000 °C and exposed to thermally activated hydrogen. The HR-EELS chamber is equipped with a Delta 0.5 spectrometer (VSI-SPECS) consisting of a double monochromator and a single analyzer housed in an UHV system with a base pressure of $\sim 8 \times 10^{-10}$ Torr. All spectra were recorded up to loss energies of 700 meV at room temperature in the specular geometry with an incident angle of 55° from the surface normal, incident energy of 5 eV and energy resolution of 5–8 meV (according to full width half maximum (FWHM) of the elastic peak).

We start with the analysis of C–H stretching mode of *as-deposited* HF CVD diamond film (grain size ~300 nm) as a function of thermal annealing. In Fig. 3, the HR-EEL spectra of the *as-deposited* HF CVD diamond sample are shown as a function of annealing temperature. While the hydrogen stretching mode is clearly present in the HR-EEL spectra of diamond up to annealing to 800 °C; annealing to 1000 °C results in its disappearance alongside with the emergence of a ~90 meV loss peak associated with C=C dimer and surface reconstruction. The detailed peak fitting procedure of C–H stretching HR-EELS mode (Fig. 3A) reveals at least three different contributions at ~350 meV, ~360 meV and ~373 meV. The first two are most likely associated with diamond (111) and (100) surfaces [14], while the last one may be attributed to sp^2-hybridised carbon [15, 16]. Upon annealing to 800 °C the maximum peak position is slightly shifted to smaller loss energies (from 359 meV to 357 meV), while the sp^2-associated mode at ~373 meV is still prominent. According to thermal stability studies of different kinds of hydrogenated amorphous carbon matrixes [17–23], annealing to a temperature of >600 °C results in desorption of hydrogen atoms alongside with hydrocarbon species, independent of the method used for amorphous carbon film preparation. This allows us to attribute the ~375 meV HR-EELS mode to hydrogen bonding to *diamond grain boundary*, which may be stable up to these high temperatures [24].

Now we turn to analyse the vibrational modes on the surface of nano-diamond films deposited by MW CVD. HR-EEL spectra of the MW-CVD-10–30 nm nano-diamond film deposited by MW CVD are shown in Fig. 4. The upper line (A) corresponds to the *as-deposited* sample followed UHV annealing to 520 °C. Spectrum 4B corresponds to the film after annealing to 800 °C. Detailed analysis of C–H stretching mode is shown in Fig. 4C and D. The Spectrum 4A is dominated by a mixed C–C stretching and C–H bending mode at 155 meV, the overtones of the diamond optical phonon at 300 meV and 450 meV, and C–H stretching vibration at 360–375 meV. Note the strong splitting of C–H stretching mode in this spectrum (Fig. 4C and D): the two maxima are positioned

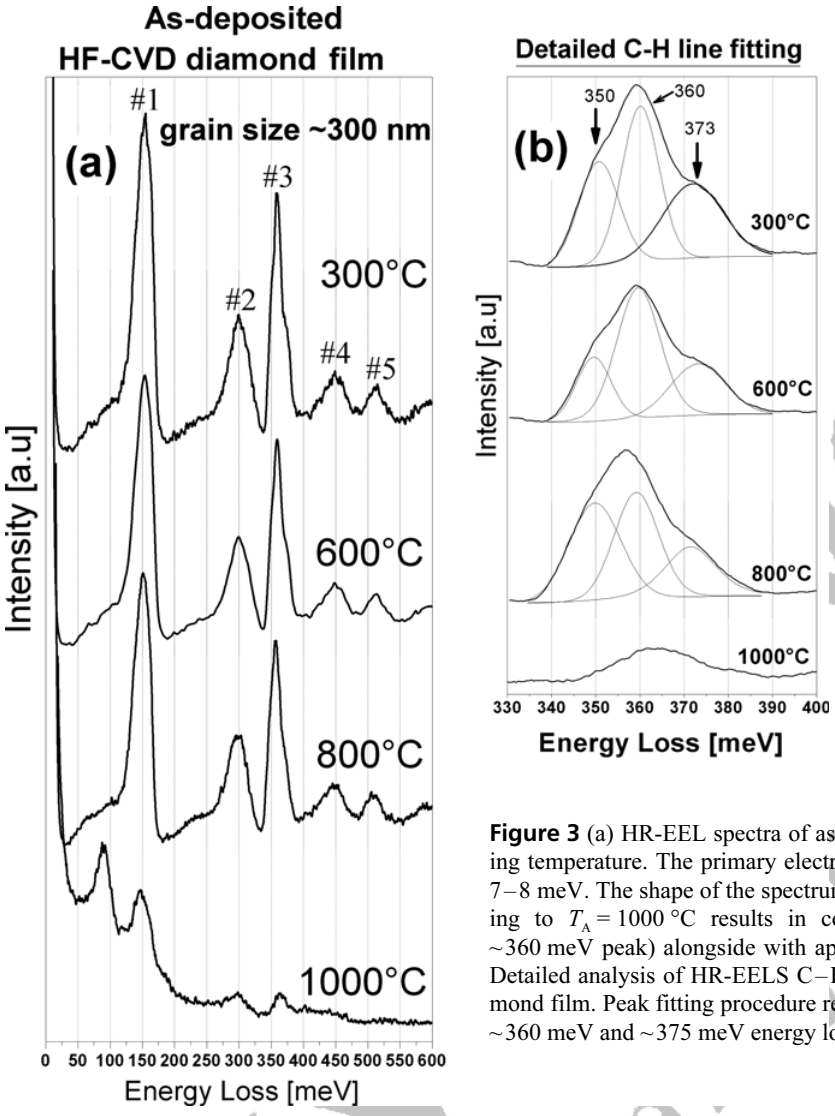

Figure 3 (a) HR-EEL spectra of as-deposited HF CVD films as function of annealing temperature. The primary electron energy was 5 eV and FWHM of elastic peak 7–8 meV. The shape of the spectrum is nearly unchanged up to T_A = 800 °C. annealing to T_A = 1000 °C results in complete hydrogen desorption (the absence of ~360 meV peak) alongside with appearance of C=C dimer mode at ~90 meV; (b) Detailed analysis of HR-EELS C–H stretching mode of as-deposited HF CVD diamond film. Peak fitting procedure reveals three different contributions at ~350 meV, ~360 meV and ~375 meV energy loss.

at ~360 meV and ~375 meV, reflecting hydrogen bonding to sp^3- and sp^2-carbon, correspondingly.

As can be seen in Fig. 3B, the HR-EEL spectrum of as-deposited HF CVD films with ~300 nm grains also display contributions at ~350 meV, ~360 meV and ~375 meV within the C–H stretching modes which are stable up to 800 °C. Obviously, the density of grain boundaries in the case of nano-diamond films exceeds that of sub-micron crystallites. Since the contribution of the ~375 meV mode is much more prominent in the case of nano-metric grains, this mode may be associated with hydrogen bonded to *diamond grain boundaries* [24]. In our studies of hydrogen adsorption on ion irradiated diamond surface [25] we concluded that nearly all kinds of hydrogenated carbon decompose near ~600 °C. This is in agreement with other studies of thermal stability of diamond like carbon which undergoes erosion/destabilization at temperature about 600 °C independently on deposition process [17–23]. The present results show that hydrogen bonded to *diamond grain boundaries* (sp^2-hybridized carbon) is stable up to temperatures of at least 800 °C. This finding allows one to distinguish the hydrogenated sp^2-hybridized carbon bonded to diamond grains from hydrogenated amorphous carbon by simple annealing procedure.

It is very interesting to note at this stage the possible correlation between the 375 meV HR-EELS mode and Raman 1140 cm^{-1} peak usually observed in the Raman spectrum of nano-diamond films: (i) both peaks are attributed to (sp^2)-carbon-hydrogen vibration; (ii) both peaks are stable up to elevated temperatures where hydrogen bonded to amorphous carbon undergoes desorption; (iii) both peaks are enhanced in the case of nano-crystalline diamond grain size. At this stage we guess that the 375 meV mode may be attributed to the stretching of the same C–H vibration, which contributes to the 1140 cm^{-1} Raman peak (currently attributed to ν_1 mode of *t*-PA) and therefore may serve as indication of nano-crystalline character of diamond films.

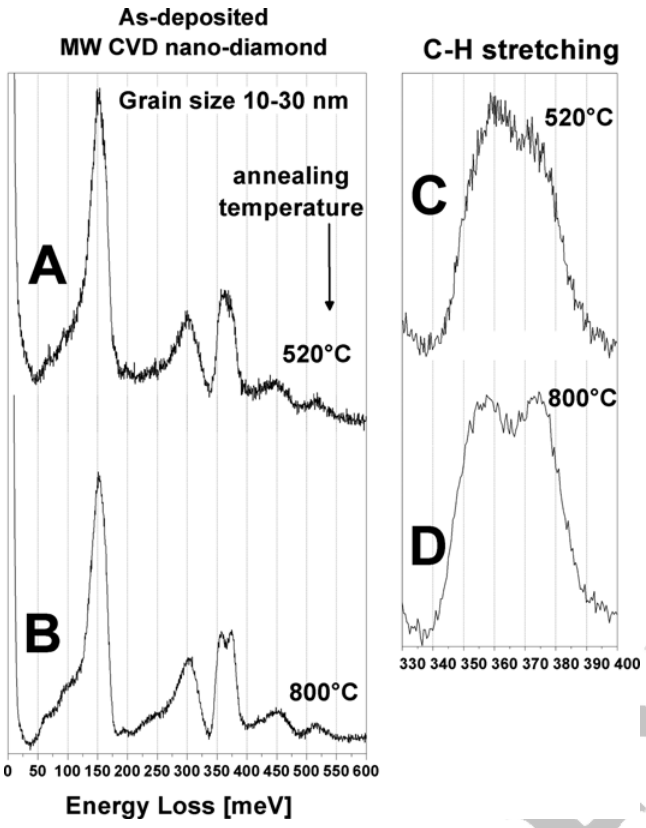

Figure 4 HR-EEL spectra of MW CVD deposited nano-diamond films: (A) as-deposited film following *in-situ* annealing to 520 °C; (B) following subsequent annealing to 800 °C. (C) and (D) Detailed analysis of HR-EELS C–H stretching mode (data originated from spectra A and B).

5 Computational study We simulated the properties of hydrogen atoms at interstitial sites at interfaces between diamond and amorphous carbon in order to have a deeper understanding of our experimental results. We compared the interstitial energy of hydrogen atoms between simulated samples of a pure diamond, amorphous carbon and within the interface between nano-diamond and amorphous carbon films.

Samples of diamond and amorphous carbon were obtained using the molecular dynamics algorithm. We also built samples with a core of nano-diamond surrounded by amorphous carbon atoms (mixed sample). Each sample had 512 carbon atoms in a (100) cubic cell with full periodic boundary conditions. The mixed sample (nano-diamond surrounded by an amorphous shell) consisted of a core of 150 atoms in a diamond structure surrounded by 362 amorphous carbon atoms. Hydrogen atoms were inserted into the mixed sample and static optimization techniques were applied to calculate the atomic configuration at the local minimum of energy. The same process was performed many times where in each case one hydrogen atom was placed at a different interstitial site. The hydrogen interstitial formation energies were plotted versus the radial distance from the interface between the diamond and the amorphous carbon. We also studied the dynamics of hydrogen atoms in the interface region by running molecular dynamics simulations on samples with many hydrogen atoms near the diamond-amorphous region.

The amorphous structure was obtained by a melt-quench process [26, 27]. The Parrinello–Rahman [28] fixed number of atoms N, pressure P, and temperature T (NPT) ensemble Molecular Dynamics (MD) algorithm with periodic boundary conditions was used to melt a 512 atoms diamond sample. Then, the same algorithm was used to cool the sample gradually until it reached equilibrium. Stillinger–Weber [29] type inter-atomic potentials, improved by Barnard–Russo [30] for tetrahedral carbon were used for the initial inter-atomic forces and energy calculations. Frauenheim's Tight Binding (FTB) model [31] was then applied to obtain the final sample atomic configuration and for the energy calculations. Then, hydrogen atoms were added to this sample and within the FTB model, Conjugate Gradient and Steepest Descent algorithms [32] were used to calculate the minimum energy configuration of the sample with the hydrogen interstitial [33].

The mixed samples were obtained by repeating the above preparation with 150 atoms in the core of the sample pinned (i.e. not allowed to move during the simulations) while the MD algorithm was applied to the other 362 atoms [34]. This process formed a nano-diamond surrounded by amorphous carbon. At the end of the formation process, a long MD simulation using the FTB model was applied to verify the stability of the sample [35]. In Fig. 5 an image of the simulated structure of the nano-diamond core with the amorphous shell is shown. This image was drawn with AViz [36]. A more detailed description of the model calculation and results will be published in the future.

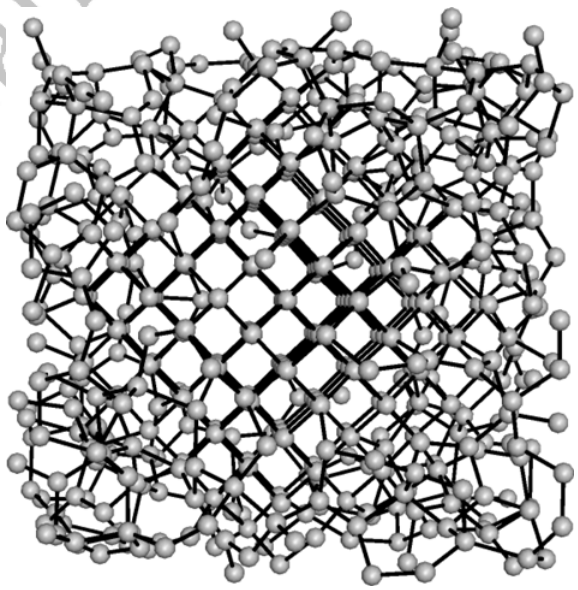

Figure 5 Simulated sample of a nano-diamond of ordered atoms surrounded by an amorphous shell.

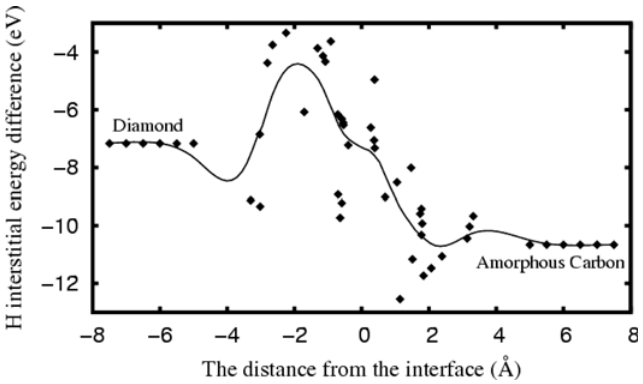

Figure 6 Total energy calculation of the nano-diamond sample with a single hydrogen atom at different interstitial sites. Each point in the plot represents a different hydrogen interstitial site, while the continuous line depicts a cubic spline interpolation. The hydrogen interstitial energies in pure diamond and in amorphous carbon samples are depicted on the left-hand side and right-hand sides of the plot, respectively.

In Fig. 6 the hydrogen interstitial energy ($E_{s\_h} - E_s$) for various interstitial sites is given. E_s denote the energy of the 512 carbon atom sample while E_{s_h} denotes the energy of the same sample with an additional hydrogen atom located in an interstitial site. The X-axis is the radial distance of the hydrogen atom from the interface between the crystalline and amorphous regions, where the interface is at $X = 0$. Each point in the plot represents a different interstitial site, where the continuous line depicts a cubic spline interpolation calculation [32]. The hydrogen interstitial energies for pure diamond and for amorphous carbon samples are depicted on the left hand side and right hand sides of the plot respectively.

From Fig. 6 we observe that: (i) the hydrogen interstitial reduces the sample energy; (ii) the hydrogen interstitial energy in the amorphous region is 3.5 eV less than the hydrogen interstitial energy in the crystalline sample; (iii) the interface creates a barrier of 3–4 eV for the diffusion of the hydrogen atoms from the crystalline to the amorphous sides of the sample; (iv) a potential well is observed in the amorphous side of the interface.

We also studied the dynamics of the hydrogen atoms in the interface region between the diamond and amorphous regions. 36 hydrogen atoms were inserted into the nano-diamond region of the mixed simulated sample described in the previous section, near the interface. Using a steepest descent algorithm with the FTB model, interstitial sites for the hydrogen atoms were obtained. Then, a molecular dynamics algorithm with the FTB model was used to raise the sample temperature to 800 °K and equilibrate the sample. During this equilibration, the 50 crystalline atoms at the center of the nano-diamond core were pinned, mimicking a sample with a larger diamond seed. If this precaution was not taken, the disorder diffuse from the amorphous region to the diamond core and eventually the whole sample became amorphous. Figure 7 shows the sample at the end

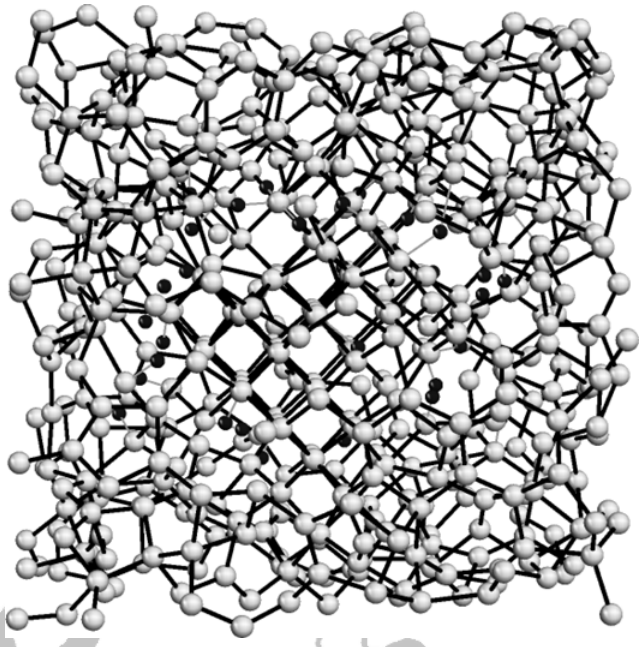

Figure 7 A mixed sample with 36 hydrogen atoms at the end of the Molecular Dynamics simulation. The gray circles depict carbon atoms, and the black small circles depict hydrogen atoms.

of the simulation where the gray circles depict the carbon atoms, and the black small circles depict hydrogen atoms.

In Fig. 8 the calculated hydrogen density distribution as a function of the hydrogen atoms distance from the center of the sample is shown at the start of the simulation and at the end of the simulation. From this distribution we observe that most of the hydrogen atoms diffused from the crystalline region to the amorphous region. The hydrogen atoms escaped from the interface region but remained close to the interface on the amorphous side. These simulation results are in agreement with the results of the previous case depicted in Fig. 6. (i) The hydrogen interstitial energy

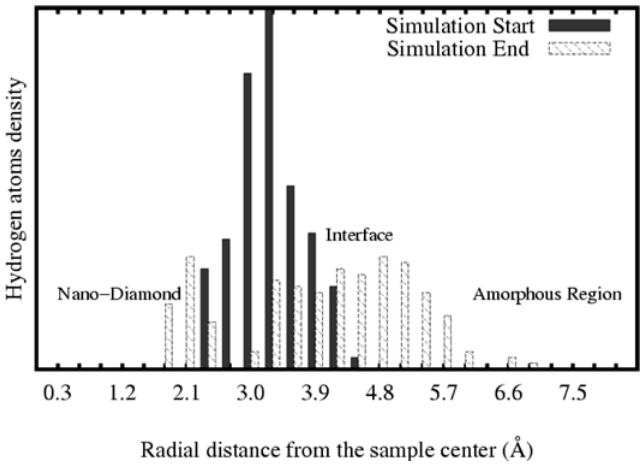

Figure 8 Distribution of the 36 hydrogen atoms in the mixed sample at the end of the Molecular Dynamics simulation as a function of the distance from the center of the sample.

at the amorphous region is lower than the hydrogen interstitial energy in the crystalline region with an energy barrier in between. (ii) There is a potential well in the amorphous region close to the interface.

6 Summary In this paper we investigated the impact of diamond grain size on the hydrogen bonding configuration and retention in poly-crystalline diamond films deposited by three different chemical vapor deposition methods. The films were grown from hydrogen rich gas mixtures (hot filament and dc GD CVD) and Ar rich/hydrogen poor gas mixture (MW CVD). SIMS studies provide direct evidence of the correlation between the concentration of hydrogen atom trapped within the films and diamond grain size, independently of deposition conditions: the smaller diamond grains result in higher hydrogen atom retention within the films. The hydrogen atoms are most likely bonded to the internal grain surfaces and within the grain boundary region to carbon atoms bonded in a predominant sp^2 configuration. Our simulations suggest that hydrogen is expected to decorate the boundaries between a nano-diamond core and an amorphous shell. Assuming that the amorphous shell may be considered similar to nano-diamond grain boundaries, our model computational studies support our experimental results and conclusions.

Acknowledgements This research project was carried out with the financial support of the Israeli Academy of Science, the Israeli Ministry of Science and Arts and the Technion Fund for promotion of research. The calculations were carried out on the Computational Physics group computers at the Technion.

References

[1] Sh. Michaelson, O. Ternyak, A. Hoffman, and Y. Lifshitz, Appl. Phys. Lett. **90**, 031914 (2007).
[2] Sh. Michaelson, O. Ternyak, R. Akhvlediani, O. A. Williams, D. Gruen, and A. Hoffman, phys. stat. sol. (a) **204**, 2860 (2007).
[3] Sh. Michaelson, O. Ternyak, R. Akhvlediani, A. Hoffman, A. Lafosse, R. Azria, O. A. Williams, and D. M. Gruen, J. Appl. Phys. **102**, 113516 (2007).
[4] Sh. Michaelson and A. Hoffman, Diam. Relat. Mater. **15**, 486 (2006).
[5] R. Akhvlediani, I. Lior, Sh. Michaelson, and A. Hoffman Diam. Relat. Mater. **11**, 545 (2002).
[6] D. Zhou, D. M. Gruen, L. C. Qin, T. G. McCauley, and A. R. Krauss, J. Appl. Phys. **84**, 1981 (1998).
[7] D. M. Gruen, Ann. Rev. Mater. Sci. **29**, 211 (1999).
[8] O. Ternyak, A. Cimmino, S. Prawer, and A. Hoffman, Diam. Relat. Mater. **14**, 272 (2005).
[9] Y. Lifshitz, Th. Kohler, Th. Frauenheim, I. Guzmann, A. Hoffman, R. Q. Zhang, X. T. Zhou, and S. T. Lee, Science **297**, 1531 (2002).
[10] Y. Lifshitz, X. M. Meng, S. T. Lee, R. Akhvlediani, and A. Hoffman, Phys. Rev. Lett. **93**, 056101 (2004).
[11] Sh. Michaelson, Y. Lifshitz, O. Ternyak, R. Akhvlediani, and A. Hoffman, Diam. Relat. Mat. **16**, 845 (2007).
[12] A. Hoffman, A. Heiman, R. Akhvlediani, E. Lakin, E. Zolotoyabko, and C. Cyterman, J. Appl. Phys. **94**, 4589 (2003).
[13] H. Ibach and D. L. Mills, Electron energy loss spectroscopy and surface vibrations (Academic, New York, 1982).
[14] T. Aizawa, T. Ando, K. Yamamoto, M. Kamo, and Y. Sato, Diam. Relat. Mater. **4**, 600 (1995).
[15] J. Ristein, R. T. Stief, L. Ley, and W. Beyer J. Appl. Phys. **84**(7), 3836 (1998).
[16] Th. Frauenheim, Th. Kohler, M. Sternberg, D. Porezag, and M. R. Pederson, Thin Solid Films **272**, 314 (1996).
[17] R. Kalish, Y. Lifshitz, K. Nugent, and S. Prawer, Appl. Phys. Lett. **74**(20), 2936 (1999).
[18] R. Kalish, in: The Physics of Diamond Int. School of Physics Enrico Fermi, Vol. 135, edited by A. Paoletti and A. Tucciarone (IOS, Amsterdam, 1997), p. 373.
[19] M. Benlahsen, B. Racine, K. Zellama, and G. Turban, J. Non-Cryst. Solids **283**, 47 (2001).
[20] Ch. Wild and P. Koidl, Appl. Phys. Lett. **51**, 1506 (1987).
[21] J. K. Walters, D. M. Fox, T. M. Burke, O. D. Weedon, R. J. Newport, and W. S. Howells, J. Chem. Phys. **101**, 4288 (1994).
[22] J. K. Walters, J. S. Rigden, R. J. Newport, S. F. Parker, and W. S. Howells, Phys. Scr. T **57**, 142 (1995).
[23] M. Lejeune, M. Benlahsen, and R. Bouzerar, Appl. Phys. Lett. **84**, 344 (2004).
[24] Sh. Michaelson, O. Ternyak, A. Hoffman, O. A. Williams, and D. M. Gruen, Appl. Phys. Lett. **91**, 103104 (2007).
[25] M. Bertin, A. Lafosse, R. Azria, Sh. Michaelson, O. Ternyak, and A. Hoffman, Appl. Phys. Lett. **90**, 061918 (2007).
[26] A. Silverman, J. Adler, and R. Weil, Thin Solid Films, **193/194**, 571 (1990).
[27] R. Zallen, in: The physics of amorphous solids (New York, Wiley-Interscience, 1983).
[28] M. Parrinello and A. Rahman, Phys. Rev. Lett. **45**, 1196 (1980); J. Appl. Phys. **52**, 7158 (1981).
[29] F. Stillinger and T. A. Weber, Phys. Rev. B **31**, 5262 (1985).
[30] A. S. Barnard and S. P. Russo, Mol. Phys. **100**(10), 1517 (2002).
[31] The Frauenheim's Tight Binding calculations were carried out using the PLATO code, see A. P. Horsfield and A. M. Bratkovsky, J. Phys.: Condens. Matter **12**, R1 (2000).
A. P. Horsfield, Phys. Rev. B **56**, 6594 (1997).
Th. Frauenheim, F. Weich, Th. Kohler, S. Uhlmann, D. Porezag, and G. Seifert, Phys. Rev. B **52**, 11492 (1995).
[32] William H. Press, Saul A. Teukolsky, William T. Vetterling, and Brian P. Flannery, Numerical Recipes, The Art of Scientific Computing (Cambridge University Press, 3rd ed. 2007).
[33] We found the hydrogen interstitial sites in diamond to be in Tetrahedral and Body Center sites, in agreement with J. P. Goss, R. Jones, M. I. Heggie, C. P. Briddon, and S. Oberg, Phys. Rev. B **65**, 115207 (2002).
D. Saada, J. Adler, and R. Kalish, Phys. Rev. B **61**, 10711 (1999).
[34] Similar preparation of pure/amorphous carbon samples was made by A. Sorkin, J. Adler, and R. Kalish, Phys. Rev. B **70**, 64110 (2004).
[35] The Radial Distribution Function (RDF) and Distribution of States (DOS) of our amorphous carbon samples are in agreements with published simulated amorphous carbon

samples, e.g. N. A. Marks, D. R. McKenzie, B. A. Pailthorpe, M. Bernasconi, and M. Parrinello, Phys. Rev. Lett. **76**, 768 (1996).
N. A. Marks, D. R. McKenzie, B. A. Pailthorpe, M. Bernasconi, and M. Parrinello, Phys. Rev. B **54**, 9703 (1996).
D. G. McCulloch, D. R. McKenzie, and C. M. Goringe, Phys. Rev. B **61**, 2349 (2000).
[36] J. Adler, J. Fox, R. Kalish, T. Mutat, A. Sorkin, and E. Warszawski, Comp. Phys. Commun. **177**, 19 (2007).